NASA Technical Memorandum 101714

Airdata Calibration of a High-Performance Aircraft for Measuring Atmospheric Wind Profiles

Edward A. Haering, Jr.

January 1990

National Aeronautics and
Space Administration

NASA Technical Memorandum 101714

Airdata Calibration of a High-Performance Aircraft for Measuring Atmospheric Wind Profiles

Edward A. Haering, Jr.
Ames Research Center, Dryden Flight Research Facility, Edwards, California

1990

National Aeronautics and
Space Administration
Ames Research Center
Dryden Flight Research Facility
Edwards, California 93523-5000

AIRDATA CALIBRATION OF A HIGH-PERFORMANCE AIRCRAFT FOR MEASURING ATMOSPHERIC WIND PROFILES

Edward A. Haering, Jr.*
NASA Ames Research Center
Dryden Flight Research Facility
Edwards, California

Abstract

The research airdata system of an instrumented F-104 aircraft has been calibrated to measure winds aloft in support of the space shuttle wind measurement investigation at the National Aeronautics and Space Administration Ames Research Center's Dryden Flight Research Facility. For this investigation, wind measurement accuracies comparable to those obtained from Jimsphere balloons were desired. This required an airdata calibration more accurate than needed for most aircraft research programs. The F-104 aircraft was equipped with a research pitot-static noseboom with integral angle-of-attack and flank angle-of-attack vanes and a ring-laser-gyro inertial reference unit. Tower flybys and radar acceleration-decelerations were used to calibrate Mach number and total temperature. Angle of attack and angle of sideslip were calibrated with a trajectory reconstruction technique using a multiple-state linear Kalman filter. The F-104 aircraft and instrumentation configuration, flight test maneuvers, data corrections, calibration techniques, and resulting calibrations and data repeatability are presented. Recommendations for future airdata systems on aircraft used to measure winds aloft are also given.

Nomenclature

Values are given in the English system of units.

Acronyms

AICS	airborne instrumentation computer system
c.g.	center of gravity
IRU	inertial reference unit
LKF	linear Kalman filter
PCM	pulse code modulation

Symbols

A	acceleration, g
A_b	normal acceleration at noseboom flow vanes, ft/sec^2
g_0	acceleration due to gravity, 32.1740 ft/sec^2
h_p	pressure altitude above mean sea level, ft
k	temperature recovery factor
M	Mach number
P_s	static pressure, lb/ft^2
P_{tot}	total pressure, lb/ft^2
p	roll rate, rad/sec
$\dot{p}$	roll acceleration, rad/sec^2
Q	calculation variable
q	pitch rate, rad/sec
$\dot{q}$	pitch acceleration, rad/sec^2
R	ideal gas constant, 53.35 $\frac{\text{ft}\cdot\text{lb}}{^\circ\text{R}\ \text{lbm}}$
r	yaw rate, rad/sec
$\dot{r}$	yaw acceleration, rad/sec^2
T	temperature, °R
u	airspeed along X axis, ft/sec
V	aircraft velocity, ft/sec
v	airspeed along Y axis, ft/sec
W	wind velocity, ft/sec
w	airspeed along Z axis, ft/sec
$\bar{x}$	distance from aircraft c.g. along aircraft X axis, ft
$\bar{\bar{x}}$	distance from flow vane along aircraft X axis, ft

*Aerospace Engineer.

$\bar{y}$	distance from aircraft c.g. along aircraft Y axis, ft
$\bar{\bar{y}}$	distance from flow vane along aircraft Y axis, ft
Z	geometric altitude above mean sea level, ft
$\bar{z}$	distance from aircraft c.g. along aircraft Z axis, ft
$\bar{\bar{z}}$	distance from flow vane along aircraft Z axis, ft

Greek

α	angle of attack, deg
β	angle of sideslip, deg
Γ	Euler rotation transformation matrix
γ	ratio of specific heats for air, 1.4
θ	pitch angle, deg
θ'	noseboom misalignment in pitch, deg
$\theta' g$	noseboom deflection in pitch due to elevated g, deg/g
ϕ	roll angle, deg
ϕ'	noseboom misalignment in roll, deg
ψ	heading angle, deg
ψ'	noseboom misalignment in yaw, deg

Superscripts

T	transpose
$\hat{}$	reference value calculated by LKF

Subscripts

1	corrected for misalignment
2	corrected for misalignment and angular rates
a	in aircraft axes
bias	Y-intercept of angle error as a function of corrected angle
c	all analytic corrections made
D	down
E	east
F	flank
fb	at fly-by tower reference altitude
I	inertial
i	indicated
m	derived by meteorlogical analysis
N	north
n	in noseboom axes
t	true
tot	total
z	Z axis accelerometer
α	angle-of-attack vane
β	flank angle-of-attack vane
∞	free stream

Introduction

The most common method of obtaining atmospheric wind profiles involves tracking a rising balloon (Jimsphere or Rawinsonde) which moves with the winds. Balloon methods are adequate for many applications but have some limitations. For example, it is impossible to control a balloon's flight path once launched. In addition, the typical rise rate is approximately 15 ft/sec (5 m/sec), so approximately an hour is required to obtain an altitude of 60,000 ft (18,000 m). For certain applications, such as the space shuttle program, it is desirable to obtain wind profiles quickly, in approximately 10 to 15 min.

The preprogrammed launch trajectory for the space shuttle is based partially on an expected wind profile for the time of year. If the winds on the day of launch are significantly different from the expected winds, certain shuttle structural load limits may be exceeded. Currently, winds are measured on the day of launch by a series of Jimsphere balloons. The last balloon for loads assessment is launched 2 hr before shuttle launch. After the balloon reaches 60,000 ft (18,000 m), the wind data are used in trajectory simulation and loads prediction programs. A wind persistence factor is added to the calculations to account for wind changes over time and the possibility that the balloon has blown away from the launch path. Studies have shown that these changes increase significantly when delays are longer than 2 hr or spatial separations are greater than 12 mi (20 km).[1–3] Depending on the results of the loads predictions, a go–no-go recommendation for launch is made.

A reduction in the uncertainties in the prelaunch wind load assessment caused by temporal and spatial variabilities was desired. The National Aeronautics and Space Administration (NASA) Johnson Space Center requested NASA Ames Research Center's Dryden Flight Research Facility to perform a flight experiment to determine the feasibility of using an instrumented high-performance aircraft to measure wind profiles. For this technique to be applicable to the space shuttle program, the following guidelines were suggested: (1) obtaining a profile to 60,000 ft (18,000 m) in 10 min, (2) an aircraft profile area within a 10 mi (16 km) radius circle, and (3) measurement accuracy comparable to the Jimsphere system. Winds are calculated as the vector difference between aircraft inertial velocity, measured by an onboard inertial reference unit (IRU) or ground based radar, and aircraft airspeed, measured by a calibrated airdata system.

The quality of the wind profiles measured by Jimsphere balloons can be shown by the tracking precision for an individual balloon and the repeatability of winds from separate balloons. Two separate radar systems' trackings show

a root-mean-square (rms) error for the Jimsphere balloon of 1.6 ft/sec (0.5 m/sec) for wind velocities averaged over 50 m intervals.[1] To match this precision, an aircraft traveling at Mach 2 would need to measure its Mach number within 0.0016 and its flow angles to within 0.05°. Studies show that the rms repeatability of wind profiles from two Jimsphere balloons is approximately 7 to 10 ft/sec (2 to 3 m/sec) if the time separation is less than 1 hr or the distance separation is less than 12 mi (20 km).[1-3] This is comparable to 0.007 to 0.010 in Mach number and 0.2° to 0.3° in flow angles at Mach 2. (Actual aircraft wind measurement repeatability depends on the accuracy of several sensors as well as on the atmospheric variability between wind measurements.) Because of these tight tolerances on Mach number and flow angles, an airdata calibration more accurate than required for most aircraft research programs is necessary.

This paper covers the methods and results of the airdata calibration of an F-104 aircraft used to measure winds aloft in support of the F-104 shuttle wind measurement investigation. Wind profile data were gathered at altitudes from 3,000 to 67,000 ft (900 to 20,400 m), Mach numbers from 0.78 to 2, angles of attack from 0° to 12°, and angles of sideslip from −3° to 3°. The F-104 aircraft and instrumentation configuration, flight test maneuvers, data corrections, calibration techniques, and resulting calibrations and data repeatabilities for Mach number, total temperature, and flow angles are presented in this report. Recommendations for future airdata systems on aircraft used to measure winds aloft are also given.

Background

Aircraft have been used to obtain wind measurements, but most results have been obtained during steady-level flight.[4-6] In steady-level flight, many simplifying assumptions are usually made. These assumptions are no longer valid in high-speed, climbing, or descending flight, as used to minimize time and spatial separation for a shuttle application. The wind measurement methods for an aircraft in a nonsteady flight environment have been documented in Ref. 7.

Traditional airdata calibration methods are well known,[8,9] but a higher accuracy than is typically achieved with these methods was desired. The methods used to achieve these accuracies are described in this report.

Description of Aircraft and Instrumentation

The aircraft used for the wind-measurement flight tests was an instrumented F-104 (Fig. 1). A standard National Advisory Committee for Aeronautics (NACA) research noseboom (Fig. 2(a)) was used to measure static and total pressures and angles of attack and sideslip.[10] Figure 2(a) also shows the size and location of the noseboom attachment collar. Indicated static pressure was measured by the forward set of static pressure orifices; the pilot's instrumentation and the aircraft airdata computer used the aft set (Fig. 2(b)). Total pressure and static pressure were each measured with a separate high-resolution, high-accuracy absolute-pressure transducer. Angle-of-attack and flank angle-of-attack values from the vanes were measured using potentiometers. Total temperature was measured by a nondeiced, open element sensor (Fig. 3). Research parameters were digitally encoded using pulse code modulation (PCM) and were both recorded onboard and telemetered to ground based recorders.

A commercial airline aircraft type ring-laser-gyro IRU was used to give inertial velocity, acceleration, attitude, and angular velocity.[11] An airborne instrumentation computer system (AICS) interfaced the IRU with the PCM system and supplied the IRU with inputs from the airdata system.[12] These inputs are needed to stabilize the IRU integration loop. Figure 4 shows the IRU, AICS, PCM system, and signal conditioning hardware installed in the aircraft.

Since the IRU was designed for commercial airline aircraft, its parameters, especially normal acceleration, were heavily low pass filtered. Because high rate maneuvers were used for the flow angle calibrations, it was decided to use a separate accelerometer set located behind the cockpit. The aircraft also had equipment which allowed trajectory guidance information to be telemetered from the ground and displayed to the pilot.[13] This guidance method is known as uplink.

Procedure

Mach Number Calibration

Mach number was calibrated using tower fly-by and radar acceleration-deceleration methods. For the tower fly-by method, shown in Fig. 5, the aircraft is flown at a steady airspeed and altitude near the fly-by tower.[9] The aircraft is sighted from the tower through an eyepiece and grid and the aircraft's true geometric altitude (Z) is determined by geometry. The free-stream static pressure at the aircraft's altitude, (P_{s_∞}) is calculated using the formula

$$P_{s_\infty} = e^{\left[\ln(P_{s_{fb}}) + \frac{g_{fb}-g}{RT_{fb}}\right]} \qquad (1)$$

where $P_{s_{fb}}$, T_{fb}, and Z_{fb}, are the static pressure, ambient air temperature, and geometric altitude at the fly-by tower reference altitude, respectively. This formula is the integral form of the hydrostatic equation.[14] The total pressure measured by the noseboom (P_{tot_i}) is assumed to be correct,[8] and the free-stream Mach number (M_∞) for subsonic flight is calculated using the expression

$$M_\infty = \sqrt{\frac{2}{\gamma - 1}\left[\left(\frac{P_{tot_i}}{P_{s_\infty}}\right)^{\frac{\gamma-1}{\gamma}} - 1\right]} \qquad (2)$$

Indicated Mach number (M_i) is calculated using equation (2) with indicated static pressure (P_{s_i}) substituted for free-stream static pressure. Passes by the tower are flown at various subsonic Mach numbers, and the Mach correction

$$\Delta M = M_\infty - M_i \qquad (3)$$

is plotted against indicated Mach number to give the Mach calibration. The calibration was assumed to be a function of indicated Mach number only, since high-lift-coefficient flight was not part of the investigation. The tower fly-by technique is the most accurate method, but only subsonic data can be taken, and only a small number of calibration points can be flown on one flight.

In the radar acceleration-deceleration technique (Fig. 6), as in the tower fly-by technique, free-stream static pressure is calculated for the aircraft. For a calibration run, the aircraft flies with wings level on a constant heading at a constant geometric altitude. The aircraft's radar altitude is uplinked to the aircraft, and the difference between the desired and actual geometric altitude is displayed in the cockpit to aid the pilot in flying a constant geometric altitude. The aircraft begins the run at a low airspeed, and accelerates at approximately 3 kn/sec to a peak Mach number. The pilot then begins to decelerate at approximately 3 kn/sec back to the original low airspeed. The entire maneuver is executed at radar elevation angles above 10° to minimize radar refraction errors and below 80° to avoid high radar antennae slew rates.[15] Time coded radar data is processed to give geometric altitude. Weather balloon and atmospheric chart data are analyzed to obtain a table of geometric altitude minus pressure altitude $(Z - hp)_m$ as a function of geometric altitude (Z). The pressure altitude error caused by lateral atmospheric pressure gradient (Δhp_m) with lateral distance and direction from the radar site is also tabulated as a function of geometric altitude. Applying these tables to the time history of the aircraft's radar altitude yields the true pressure altitude of the aircraft, which is then converted into free-stream static pressure.[16] As with the tower fly-by method, indicated total pressure is assumed to be true in subsonic flight, and only normal shock losses are assumed in supersonic flight.[8] Equation (2) is then used to calculate free-stream Mach number subsonically, (when $P_{tot_i}/P_{s_\infty} < 1.89293$, the value at $M_\infty = 1.0$).

where

$$Q = 1.839371\left(\frac{P_{s_\infty}}{P_{tot_i}}\right)$$

is used supersonically, (when $P_{tot_i}/P_{s_\infty} > 1.89293$). This equation is a Taylor series expansion of the Raleigh pitot-static equation.[16] Indicated Mach number is calculated by using equations (2) and (4) with indicated static pressure replacing free-stream static pressure. As with the tower fly-by data, equation (3) is used to obtain the Mach correction. The result is plotted against indicated Mach number. The radar acceleration-deceleration method is useful because: (1) it allows supersonic Mach calibration, (2) it is independent of the tower fly-by method, (3) the entire Mach calibration can be obtained in a few minutes of flight time, and (4) the maneuvers can be conducted at several altitudes to check for altitude effects on calibration.

The radar acceleration-deceleration Mach corrections are inconsistent with those derived by the tower fly-by method. This difference in Mach correction is a pure bias in altitude. Compared to the tower fly-by method, the pressure altitude derived from radar and weather analysis is too low. The locus of points, obtained on days when the atmosphere was relatively calm, has a generally increasing magnitude of altitude bias with increasing altitude. The bias ranges from 0 error near the ground to as much as −264 ft at a pressure altitude of 34,000 ft. The cause of this altitude bias is being investigated, but is thought to be a systematic error in the measurement or analysis of the weather or radar data.

The altitude bias error in the radar acceleration-deceleration data was eliminated by "bootstrapping." For this technique, the indicated Mach number for a single, subsonic point at the beginning of the acceleration is calculated. The pressure altitude is calculated using the Mach calibration derived from a tower fly-by. The difference between this pressure altitude and that calculated from radar and the $(Z - hp)_m$ and Δhp_m tables from the weather analysis is the altitude bias. The altitude bias correction is then applied to the entire maneuver. The correction is valid as long as the maneuver is flown at a nearly constant altitude. The resulting calibration agrees well with the tower fly-by calibration over the entire subsonic Mach range, even though only one point of the radar acceleration-deceleration calibration was forced equal to the tower fly-by calibration. At a given Mach number the aircraft altitude is correlated to the aircraft angle of attack. Since the static pressure measured by a standard NACA airdata probe is insensitive to angles of attack up to 20°,[10] the aircraft's Mach number calibration should not depend on

$$M_\infty = \sqrt{\frac{1.42857 - 0.357143Q - 0.0625Q^2 - 0.025Q^3 - 0.012617Q^4 - 0.00715Q^5 - 0.0043458Q^6 - 0.0087725Q^9}{Q}} \qquad (4)$$

angle of attack, or thereby altitude. Therefore, the Mach number calibration should not be a function of the altitude bias correction.

Total Temperature Calibration

The ambient air temperature at the aircraft altitude (T_∞) may be calculated from the measured total temperature (T_{tot}), and free-stream Mach number by

$$T_\infty = \frac{T_{tot}}{1 + \frac{\gamma-1}{2} k M_\infty^2} \tag{5}$$

where k is the recovery factor of the total temperature sensor. The value of k is usually a constant parameter and is dependent on the sensor geometry. The recovery factor can be calculated using tower fly-by and radar acceleration-deceleration data. If total temperature is plotted as a function of free-stream Mach number squared, the slope is $\frac{\gamma-1}{2} T_\infty k$, and the y-intercept is the free-stream temperature. A least-squares curve fit was used to determine these quantities (Fig. 7). The value of the recovery factor for the aircraft is taken to be the average from all the maneuvers analyzed.

Flow Angle Corrections

The vanes on the noseboom measure the angles between the local velocity vector and the noseboom axes. Figure 8 shows the steps taken to correct these angles to true angles of attack and sideslip: (1) noseboom misalignment correction, (2) aircraft angular-rate correction, (3) noseboom bending correction, (4) aerodynamic flow angle calibration correction, and (5) transformation of flank angle of attack to angle of sideslip. The first, second, third, and fifth steps are analytical corrections. The fourth is determined through trajectory reconstruction techniques. Figure 9 shows the difference between flank angle of attack and angle of sideslip.

Noseboom Misalignment Corrections. The first correction to the flow angles (Fig. 8) is for noseboom misalignment. The noseboom on an aircraft may be imperfectly aligned with the aircraft axes. To transform the angles from the noseboom axes system (X_n, Y_n, and Z_n) to the aircraft axes system (X_a, Y_a, and Z_a) (Fig. 10), the three components of the true airspeed in the noseboom axes system (u_n, v_n, and w_n) must be calculated. The free-stream velocity (in ft/sec) is calculated by

$$V_\infty = M_\infty \sqrt{\gamma R g_0 T_\infty} \tag{6}$$

The three components of airspeed are then evaluated

$$u_n = \frac{V_\infty}{\sqrt{1 + \tan^2(\alpha_i) + \tan^2(\alpha_{F_i})}} \tag{7}$$

$$v_n = u_n \tan(\alpha_{F_i})$$

$$w_n = u_n \tan(\alpha_i)$$

where α_i is the indicated angle of attack and α_{F_i} is the indicated flank angle of attack. The angular offset of the noseboom in roll (ϕ'), pitch (θ'), and yaw (ψ') is measured from the aircraft axes to the noseboom axes (Fig. 10). An Euler rotation through these angles transforms the noseboom axes (u_n, v_n, and w_n) components into the aircraft axes (u_a, v_a, and w_a)

$$\begin{bmatrix} u_a \\ v_a \\ w_a \end{bmatrix} = \Gamma \begin{bmatrix} u_n \\ v_n \\ w_n \end{bmatrix} \tag{8}$$

where

$$\Gamma = \begin{bmatrix} \cos(\psi') & -\sin(\psi') & 0 \\ \sin(\psi') & \cos(\psi') & 0 \\ 0 & 0 & 1 \end{bmatrix} \times \begin{bmatrix} \cos(\theta') & 0 & \sin(\theta') \\ 0 & 1 & 0 \\ -\sin(\theta') & 0 & \cos(\theta') \end{bmatrix} \times \begin{bmatrix} 1 & 0 & 0 \\ 0 & \cos(\phi') & -\sin(\phi') \\ 0 & \sin(\phi') & \cos(\phi') \end{bmatrix}$$

The indicated angle of attack and flank angle of attack can be expressed in the aircraft axes system by

$$\alpha_1 = \tan^{-1}\left(\frac{w_a}{u_a}\right)$$
$$\alpha_{F_1} = \tan^{-1}\left(\frac{v_a}{u_a}\right) \tag{9}$$

The axes system transformation was necessary because of the high accuracy of the angle-of-attack and -sideslip measurements needed to accurately measure winds. At an angle of attack of 20° and an angle of sideslip of 5°, on this aircraft, neglecting the noseboom misalignment correction would result in a 0.5°-error in flow angle.

To measure the boom offset angles for roll, pitch, and yaw a clinometer and transit are used. The roll and pitch attitude of the aircraft are measured with the clinometer at reference points on the aircraft in the hangar. The clinometer is then used to measure the pitch and roll angles of the noseboom, taking into account the 0.33°-taper in the support shaft of the angle-of-attack vane. The differences are the angular offset for roll and pitch respectively. The yaw offset angle is determined by sighting two hard points on the aircraft and two points on the noseboom using the transit.

The noseboom is fastened to the aircraft radome, which is removed periodically for maintenance. After removing and reinstalling the radome, the boom misalignment measurement is repeated. The values for the offset angles for two flight periods are given in Table 1. These quantities vary by a significant amount.

Aircraft Angular-Rate Corrections. The second correction to the flow angles (Fig. 8) is for angular rates of the aircraft. As the aircraft rolls, pitches, and yaws, the motion

of the noseboom about the center of gravity (c.g.) induces additional airspeed components, deflecting the flow vanes. For angle of attack, the pitching and rolling effects of the aircraft were accounted for by

$$\alpha_2 = \alpha_1 + \sin^{-1}\left(\frac{(q\bar{x}_\alpha - p\bar{y}_\alpha)\cos(\alpha_1)}{V_\infty}\right) \quad (10)$$

where p, q, and r are the aircraft roll, pitch, and yaw rates, respectively, and $\bar{x}_\alpha$ and $\bar{y}_\alpha$ are the longitudinal and lateral distances from the aircraft c.g. to the angle-of-attack vane. These distances are tabulated in Table 2. For flank angle of attack, rolling and yawing effects are accounted for by

$$\alpha_{F_c} = \alpha_{F_1} + \sin^{-1}\left(\frac{(p\bar{z}_\beta - r\bar{x}_\beta)\cos(\alpha_{F_1})}{V_\infty}\right) \quad (11)$$

where $\bar{z}_\beta$ and $\bar{x}_\beta$ are the normal and longitudinal distances from the aircraft c.g. to the flank angle-of-attack vane. These are also given in Table 2. Figure 11 shows the angular-rate corrections. Equations (10) and (11) are not limited by small angle approximations and are applicable to high angle-of-attack and high angle-of-sideslip calculations.

These angular rates, like other parameters measured by the IRU, have time delays and need to be skewed the appropriate amount in time. The time delays for this configuration are shown in Table 3.

Noseboom Bending Correction. The third flow angle correction (Fig. 8) is for noseboom bending. During elevated-g maneuvering, the noseboom deflects under the increased load. The noseboom deflection in pitch caused by elevated g (θ'_g) was measured experimentally for this aircraft as $-0.064°/g$. No correction is made for noseboom bending in the yaw plane, since the aircraft is not significantly loaded in that plane.

The aircraft's accelerometer package is located behind the cockpit in the electrical bay, so acceleration data must be translated to the noseboom before the noseboom deflection can be calculated. Table 2 presents the distances $\bar{\bar{x}}_z$, $\bar{\bar{y}}_z$, and $\bar{\bar{z}}_z$, from the noseboom to the vertical accelerometer (A_z). The normal acceleration at the noseboom (A_b) is

$$A_b = -A_z + \frac{(pr - \dot{q})\bar{\bar{x}}_z + (qr + \dot{p})\bar{\bar{y}}_z - (p^2 + q^2)\bar{\bar{z}}_z}{g_0} \quad (12)$$

The roll, pitch, and yaw accelerations ($\dot{p}$, $\dot{q}$, and $\dot{r}$) were numerically differentiated from p, q, and r using a five point weighted least-squares sliding window.[17]

Angle of attack corrected for noseboom bending is

$$\alpha_c = \alpha_2 - \theta'_g(A_b - \cos(\theta)\cos(\phi)) \quad (13)$$

where the term involving the cosines subtracts the normal acceleration caused by gravity.

Aerodynamic Flow Angle Calibrations Corrections. The fourth correction to the flow angles (Fig. 8) is for aerodynamic effects that the aircraft and the noseboom induce on the local velocity vector. These effects have been calibrated through flight test data using a trajectory reconstruction algorithm. The corrections for angle of attack will be called upwash and for flank angle of attack the corrections will be called sidewash.

For subsonic flight, upwash was identified using the following flight test technique. Aided by the uplink, the pilot held the aircraft at a constant altitude, Mach number, and power setting for several seconds, then swept through a range of angle of attack, followed by several seconds of stabilized data (Fig. 12(a)). Sidewash was calibrated in a similar fashion with sweeps in flank angle of attack (Fig. 12(b)). These maneuvers were conducted at true Mach numbers ranging from 0.78 to 0.92.

Since no flow disturbances from the aircraft can propagate forward to the flow vanes in supersonic flow, upwash and sidewash will not be a function of angle of attack or flank angle of attack. Shock waves on the noseboom affect the indicated flow angles however, so upwash and sidewash are identified as a function of indicated Mach number, using the radar acceleration-deceleration maneuver described earlier.

The true angle of attack and flank angle of attack are calculated by a trajectory reconstruction algorithm with a multiple-state linear Kalman filter (LKF).[18] The LKF blends data from the aircraft's accelerometers, IRU, airdata system, radar tracking, and weather analysis to give the minimum variance estimate of the aircraft's trajectory. The observations and the dynamics equations are selectively weighted using a matrix determined by physical intuition about the system. Tables 4 and 5 give the observation weighting matrixes used for the upwash and sidewash calibrations. Tables 6 and 7 show the weightings used for the dynamics equations. The LKF algorithm consists of a prediction and a correction step. The prediction step extrapolates the measured data to the next time point using the dynamics equations. The correction step adjusts the extrapolated state using measured data at that next time point to give the minimum variance estimate.[18]

The components of the inertial velocity and winds aloft, calculated by the LKF, were added in vector form to give estimates of true angle of attack and flank angle of attack for each time point in the calibration maneuver, that is at each data frame. True angle of attack and true flank angle of attack are determined from the LKF reference states as

$$\alpha_t = \tan^{-1}\left[\frac{\hat{w}}{\hat{u}}\right] \quad (14)$$

$$\alpha_{F_t} = \tan^{-1}\left[\frac{\hat{v}}{\hat{u}}\right] \quad (15)$$

where

$$\begin{bmatrix}\widehat{u}\\ v\\ w\end{bmatrix} = \Gamma^T\left\{\begin{bmatrix}\widehat{V_N}\\ V_E\\ V_D\end{bmatrix} - \begin{bmatrix}\widehat{W_N}\\ W_E\\ W_D\end{bmatrix}\right\}$$

$$\Gamma^T = \begin{bmatrix} 1 & 0 & 0 \\ 0 & \cos(\phi) & \sin(\phi) \\ 0 & -\sin(\phi) & \cos(\phi) \end{bmatrix} \times \begin{bmatrix} \cos(\theta) & 0 & -\sin(\theta) \\ 0 & 1 & 0 \\ \sin(\theta) & 0 & \cos(\theta) \end{bmatrix} \times \begin{bmatrix} \cos(\psi) & \sin(\psi) & 0 \\ -\sin(\psi) & \cos(\psi) & 0 \\ 0 & 0 & 1 \end{bmatrix} \quad (16)$$

There are several things to note in these equations. First, true flank angle of attack is used since it is independent of angle of attack and more directly comparable to corrected flank angle of attack than true angle of sideslip is. Second, the vertical component of the wind measurement is set to zero since it is difficult to measure using weather balloons. Lastly, Γ^T is used to transform the velocity components from earth axes to aircraft body axes.

The errors in angle of attack and flank angle of attack are

$$\Delta\alpha = \alpha_c - \alpha_t \quad (17)$$

$$\Delta\alpha_F = \alpha_{F_c} - \alpha_{F_t} \quad (18)$$

These errors are plotted as functions of corrected angle of attack, corrected flank angle of attack, and indicated Mach number in order to identify systematic trends that can be used for a calibration. Figure 13 shows typical subsonic calibration maneuvers at a free-stream Mach number of 0.92. Once identified, a line is fit to the data using least-squares regression. The slope of the error in angle of attack as a function of corrected angle of attack curve $\left(\frac{\delta\Delta\alpha}{\delta\alpha_c}\right)$ is defined as the upwash factor, and the slope of the error in flank angle of attack as a function of corrected flank angle of attack curve $\left(\frac{\delta\Delta\alpha_F}{\delta\alpha_{F_c}}\right)$ is the sidewash factor. The y-intercepts of the curves are the angle-of-attack and flank angle-of-attack biases (α_{bias} and $\alpha_{F_{bias}}$). The upwash and sidewash factors are a function of indicated Mach number as is the angle-of-attack bias.

No trend of flank angle-of-attack bias with indicated Mach number was found in this calibration. The high sensitivity of flank angle of attack to small changes in the wind estimate makes this task impossible without many more data flights to get a statistically significant set of data points. This is a limitation of the method since it relies on an accurate measurement of the winds by weather balloons.

Subsonically, the true angle of attack and true flank angle of attack are calculated by

$$\alpha_t = \alpha_c - \left[\frac{\delta\Delta\alpha}{\delta\alpha_c}\alpha_c + \alpha_{bias}\right] \quad (19)$$

$$\alpha_{F_t} = \alpha_{F_c} - \left[\frac{\delta\Delta\alpha_F}{\delta\alpha_{F_c}}\alpha_{F_c} + \alpha_{F_{bias}}\right] \quad (20)$$

for $M_i < 1.0$.

As noted previously, in supersonic flight flow angle errors are a function of Mach number only. The trend with Mach number is continuous and repeatable outside of the transonic region, where local shock waves interfere with the flow vanes.[19] True angle of attack and true flank angle of attack for supersonic flight are

$$\alpha_t = \alpha_c - \Delta\alpha \quad (21)$$

$$\alpha_{F_t} = \alpha_{F_c} - \Delta\alpha_F \quad (22)$$

for $M_i > 1.0$.

The calibration coefficients can be used as long as the external configuration of the aircraft is not significantly altered and the sensors have not degraded. It is important to have preflight inspections of the noseboom, total temperature sensor, IRU, and supporting electronics to assure quality data will be gathered.

Transformation of Flank Angle of Attack to Angle of Sideslip. The fifth and last correction to the flow angles (Fig. 8) is the transformation of flank angle of attack to angle of sidelip, given by

$$\beta_t = \tan^{-1}\left[\tan(\alpha_{F_t})\cos(\alpha_t)\right] \quad (23)$$

The distinction between these two angles is shown in Fig. 9.

Results and Discussions

Mach Number Calibration

To calibrate Mach number for this aircraft, 22 tower fly-by points and 11 radar acceleration-deceleration maneuvers were obtained and analyzed. Figure 14 shows the Mach number calibration correction as a function of indicated Mach number for all the calibration maneuvers. All of the radar acceleration-deceleration data were corrected using the bootstrap technique. As Fig. 14 shows, the scatter is approximately ± 0.003 in the subsonic data, and approximately ± 0.005 in the supersonic data. A curve faired through the data was used as the Mach number calibration, shown in Fig. 14 as a solid line.

Total Temperature Calibration

Total temperature was calibrated by extracting the recovery factor from tower fly-by and radar acceleration-deceleration data. Table 8 shows the individual recovery factors with magnitudes varying from 0.977 to 0.995, with an average of 0.986. Some of the ± 0.009 scatter is caused by variations in ambient air temperature during the calibration maneuvers, especially for the tower fly-by maneuvers which were conducted over more than an hour of flight time. Wind-tunnel data for this type of temperature sensor yields recovery factors between 0.992 and 0.999.[20]

Flow Angle Calibrations

The flow angles for this aircraft were corrected using the five steps shown in Fig. 8. One of these steps was correcting the flow angles for aerodynamic upwash and sidewash.

Subsonic Upwash Calibration. Figure 15 shows the subsonic upwash factor as a function of indicated Mach number. The increase of the upwash factor with increasing Mach number is thought to be caused by a compression effect on the angle-of-attack vane, caused by the close proximity to the flank angle-of-attack vane support shaft. Dual flank angle-of-attack vanes, one opposite the original vane, would make the compression field symmetrical about the $X_n - Y_n$ plane, and negate the change in upwash factor with indicated Mach number. The dependance of the angle-of-attack bias on indicated Mach number is shown in Fig. 16, along with its calibration fairing. Comparing the fully calibrated subsonic angle of attack with the LKF estimate yields a residual bound of approximately $\pm 0.2°$.

Subsonic Sidewash Calibration. The subsonic sidewash factor plotted as a function of indicated Mach number is shown in Fig. 17. The increase in sidewash factor with increasing Mach number above $M_i = 0.84$ is thought to be caused by a compression effect on the flank angle-of-attack vane caused by the noseboom attachment collar located immediately behind the vane (Fig. 2(a)). The flank angle-of-attack bias had too much scatter to calibrate because of its high sensitivity to errors in the meteorological winds estimate. For these calibrations, the flank angle-of-attack bias was assumed to be zero. Comparing the fully calibrated subsonic flank angle of attack with its LKF reference estimate yields a residual whose variations about the mean are bounded by $\pm 0.15°$, meaning sidewash factor has been calibrated to within $\pm 0.15°$.

Supersonic Upwash Calibration. Figure 18 shows the supersonic angle-of-attack error as a function of indicated Mach number for several flights with its faired calibration curve. The calibration curve shows a sharp drop in error at $M_i = 1.20$, which is thought to be caused by a local shock wave crossing the angle-of-attack vane. At higher indicated Mach numbers, angle-of-attack error is constant. As Fig. 18 shows, the flight-to-flight scatter in the supersonic angle-of-attack calibration is approximately $\pm 0.3°$.

Supersonic Sidewash Calibration. Figure 19 shows the supersonic flank angle-of-attack error as a function of indicated Mach number for several flights along with its faired calibration curve. The decrease in the change in flank angle of attack above $M_i = 1.250$ is thought to be caused by the single angle-of-attack vane. The oblique shock wave off of the angle-of-attack vane and support shaft increases the static pressure on the port side of the noseboom, making the flank angle-of-attack vane read too low. This effect becomes more pronounced as indicated Mach number increases because of the increasing shock strength, as the curve's negative slope shows. Dual angle-of-attack vanes would make the pressure distribution around the noseboom symmetric about the $X_n - Z_n$ plane, negating the Mach effect on flank angle of attack. As Fig. 19 shows, the flight-to-flight scatter in the supersonic flank angle-of-attack calibration is approximately $\pm 0.25°$.

Effect of Airdata Calibration on Wind Measurement Quality

Assuming negligible errors in the inertial velocities calculated by the IRU or ground based radar, the calibration repeatabilities attained should result in measured wind speed repeatabilities of 3 to 10 ft/sec (1 to 3 m/sec). The airdata repeatabilities, in terms of the calibration error bounds, are similar to the rms repeatability as the radar tracked Jimsphere balloon.[1-3] The wind speed repeatability of 3 ft/sec is calculated assuming a Mach number of 0.9, and the 10 ft/sec repeatability assumes a Mach number of 2. Since the flow angles are used to resolve the airspeed into wind components, a given error in a flow angle will cause an increasing wind error as aircraft speed increases. For this aircraft high speeds, however, are necessary to obtain high altitudes and to rapidly survey the altitude desired.

Recommendations

Several recommendations from this experiment may be helpful in the design and operation of future airdata systems for aircraft used to measure winds aloft. To minimize the effects of Mach number on the flow angles, dual vanes for both angle of attack and flank angle of attack should be used, making the flow field symmetrical vertically and laterally. Increasing the distance between the sets of angle-of-attack vanes and flank angle-of-attack vanes should reduce the compression effect on the vanes, and eliminating the noseboom attachment collar will eliminate any compression effect on the flank angle-of-attack vanes.

On this program, problems were encountered with the flow angle potentiometers, which changed calibrations as they wore. The angle sensing elements of a syncro angle transducer do not rub against each other, and would not be susceptible to this problem.

Since an accurate knowledge of the angular offset of the noseboom from the IRU is necessary for a successful calibration, these two systems should be rigidly attached to the same structure. The structure should have a location to measure externally roll, pitch, and yaw angles on the ground. This would minimize the effects of maintenance and aircraft bending and torsion in flight on the misalignment angles.

Concluding Remarks

The research airdata system of an F-104 aircraft has been calibrated to measure winds aloft. The wind measurement accuracy desired for this investigation required an airdata calibration more accurate than for most aircraft research programs. Mach number was calibrated using the tower fly-by and radar acceleration-deceleration techniques, with a flight-to-flight calibration repeatability of ± 0.003 subsonically and ± 0.005 supersonically. Total temperature was calibrated and found to have a recovery factor of 0.986 with a ± 0.009 scatter in the data.

Flow angles were corrected for noseboom misalignment, time delays, aircraft angular rates, and noseboom

bending, then calibrated using trajectory reconstruction using a multiple state linear Kalman filter (LKF). Noseboom misalignment was corrected by an Euler rotation through its offset angles. The flow angles were corrected for aircraft angular rates without using small angle approximations.

The trajectory reconstruction calibration method using the multiple-state LKF allows several different data sources to be blended, minimizing systematic errors in the data and yielding highly accurate trajectory information. The flight-to-flight calibration repeatability of angle of attack is $\pm 0.2°$ subsonically and $\pm 0.3°$ supersonically, and the flight-to-flight calibration repeatability of flank angle of attack is $\pm 0.15°$ subsonically and $\pm 0.25°$ supersonically. These calibration repeatabilities are considered to be near the attainable accuracy limit with the configuration used. The subsonic flank angle-of-attack bias data had too much scatter to calibrate, probably because of the high sensitivity of the true flank angle-of-attack calculation to small errors in the meteorological wind estimate.

Assuming negligible errors in the inertial velocities calculated by the inertial reference unit (IRU) or ground based radar, the airdata calibration repeatabilities attained should result in measured wind speed repeatabilities of 3 to 10 ft/sec (1 to 3 m/sec), approximately the same repeatability as the radar tracked Jimsphere balloon.

Several recommendations from this investigation will be useful in the design and operation of future airdata systems for aircraft used to measure winds aloft. These include using a noseboom with dual angle-of-attack and flank angle-of-attack vanes to reduce the sensitivity of upwash and sidewash on Mach number. The noseboom and IRU should be rigidly attached to the same structure to minimize geometric alignment variability.

References

[1] Hill, Charles K., *Analysis of Jimsphere Pairs for Use in Assessing Space Vehicle Ascent Capability*, NASA TP-2573, 1986.

[2] Adelfang, S.I., *Study of Wind Change for the Development of Loads Reduction Techniques for the Space Shuttle*, NASA CR-4045, 1987.

[3] Wilfong, Timothy L., and Boyd, Billie F., "Winds Aloft to Support Space and Missile Launches," *Proceedings of the Third International Conference on the Aviation Weather System*, Anaheim, CA, Jan. 3–Feb. 3, 1989, pp. 102–107.

[4] Lenschow, Donald H., *Probing the Atmospheric Boundary Layer*, American Meteorological Society, Boston, MA, 1986, pp. 39–55.

[5] Ritter, J., Beck, S., Hedgepeth, R., and Barrick, J., "The Development of an Air Motion Measurement System for NASA's Electra Aircraft," Sixth Symposium on Meteorological Observations and Instrumentation, New Orleans, LA, Jan. 12–16, 1987.

[6] Schänzer, G., Swolinsky, M., and Vörsmann, P., "Flight Test Equipment for the On-board Measurement of Wind Turbulence," AGARD Report No.734, June 1988. Presented at the 65th Meeting of the Structures and Materials Panel, Cesme, Turkey, Oct. 4–9, 1987.

[7] Bjarke, Lisa J., and Ehernberger, L.J., *An In-Flight Technique for Wind Measurement in Support of the Space Shuttle Program*, NASA TM-4154, 1989.

[8] Gracey, William, *Measurement of Aircraft Speed and Altitude*, NASA RP-1046, May, 1980.

[9] De Anda, Albert G., "AFFTC Standard Airspeed Calibration Procedures," AFFTC-TIH-81-5, June, 1981.

[10] Richardson, Norman R., and Pearson, Albin O., *Wind-Tunnel Calibrations of a Combined Pitot-Static Tube, Vane-Type Flow-Direction Transmitter, and Stagnation-Temperature Element at Mach Numbers from 0.60 to 2.87*, NASA TN D-122, 1959.

[11] Litton Aero Products, LTN-90 *Inertial Reference Unit Component Maintenance Manual*, 34-47-01, Revision 8, June, 1986.

[12] Bever, Glenn A., *The Development of an Airborne Instrumentation Computer System for Flight Test*, NASA TM-86036, 1984.

[13] Meyer, R.R., Jr., Schneider, Cdr. E.T., "Real-Time Pilot Guidance System For Improved Flight Test Maneuvers," AIAA-83-2747, Nov., 1983.

[14] National Oceanic and Atmospheric Administration, National Aeronautics and Space Administration, United States Air Force, *U.S. Standard Atmosphere*, 1976.

[15] James, Robert, and Brownlow, James D., *Mathematical Analysis Study for Radar Data Processing and Enhancement Part II: Modeling of Propagation Path Errors*, NASA CR-166616, 1985.

[16] Johnson, J. Blair, Larson, Terry J., and Ficke, Jules M., *Digital Program for Calculating Static Pressure Position Error*, NASA TM-86726, 1987.

[17] Carnahan, Brice, Luther, H.A., and Wilkes, James O., *Applied Numerical Methods*, John Wiley & Sons, New York, 1969.

[18] Whitmore, Stephen A., Larson, Terry J., and Ehernberger, L.J., *Air Data Position-Error Calibration Using State Reconstruction Techniques*, NASA TM-86029, 1984.

[19] Sakamoto, Glenn M., *Aerodynamic Characteristics of a Vane Flow Angularity Sensor System Capable of Measuring Flightpath Accelerations For the Mach Number Range From 0.40 to 2.54*, NASA TN D-8242, 1976.

[20] Stickney, Truman M., Shedlov, Marvin W., Thompson, Donald I., and Yakos, Frank T., *Rosemount Total Temperature Sensors*, Technical Report 5755, Revision A, 1981.

Table 1. Noseboom misalignment.

Flight Period	ϕ', deg	θ', deg	ψ', deg
Check 1	−1.33	−0.40	0.53
Check 2	−1.25	−0.23	0.27

Table 2. Sensor transformation distances.

Parameter	Distance from c.g., ft	Distance from noseboom to accelerometer, ft
$\bar{x}_\alpha$	35.12	
$\bar{y}_\alpha$	−0.57	
$\bar{x}_\beta$	34.77	
$\bar{z}_\beta$	1.09	
$\bar{x}_z$		−20.15
$\bar{y}_z$		0.2552
$\bar{z}_z$		−1.130

Table 3. Time delays for IRU.

Parameter	Time delay, sec
ϕ	0.050
θ	0.050
ψ	0.110
p	0.050
q	0.050
r	0.050
True ground speed	0.110
True ground track angle	0.110
Flight path angle	0.110
V_D	0.065

Table 4. Angle-of-attack observation weights.

	Weighting		
Measurement	North	East	Down
Aircraft position	10	10	10
Inertial velocity	100	100	100
Winds	10	10	0.001
	Indicated	Meteorological	M_i
Pressure	1	1	1
	T_{tot}	Meteorological	
Temperature	2	1	

Table 5. Flank angle-of-attack observation weights.

	Weighting		
Measurement	North	East	Down
Aircraft position	10	10	10
Inertial velocity	1000	1000	1000
Winds	10	10	10
	Indicated	Meteorological	M_i
Pressure	1	2	2
	T_{tot}	Meteorological	
Temperature	5	1	

Table 6. Angle-of-attack dynamic equations weights.

	Weighting		
Measurement	North	East	Down
Aircraft position	100	100	100
Inertial velocity	100	100	100
Winds	1	10	10,000
	Ambient	Mach	Position error
Pressure	1	1	1
	Ambient		
Temperature	1		

Table 7. Flank angle-of-attack dynamic equations weights.

	Weighting		
Measurement	North	East	Down
Aircraft position	10	10	10
Inertial velocity	10	10	10
Winds	200	200	10,000
	Ambient	Mach	Position error
Pressure	1	1	1
	Ambient		
Temperature	1		

Table 8. Total temperature recovery factor calibrations.

Maneuver	Recovery factor, k
1	0.9897
2	0.9953
3	0.9913
4	0.9766
5	0.9786
Average k	0.986

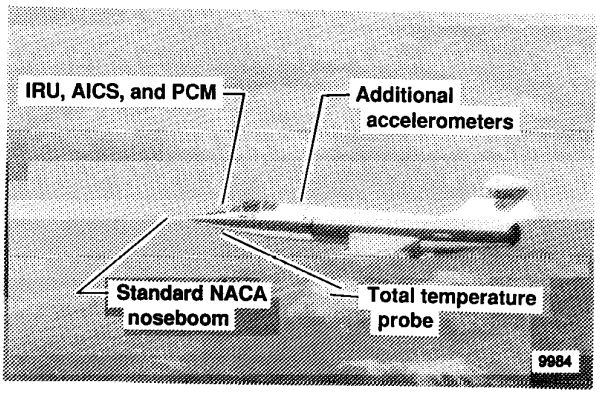

EC88-0009-004

Fig. 1 The F-104 aircraft.

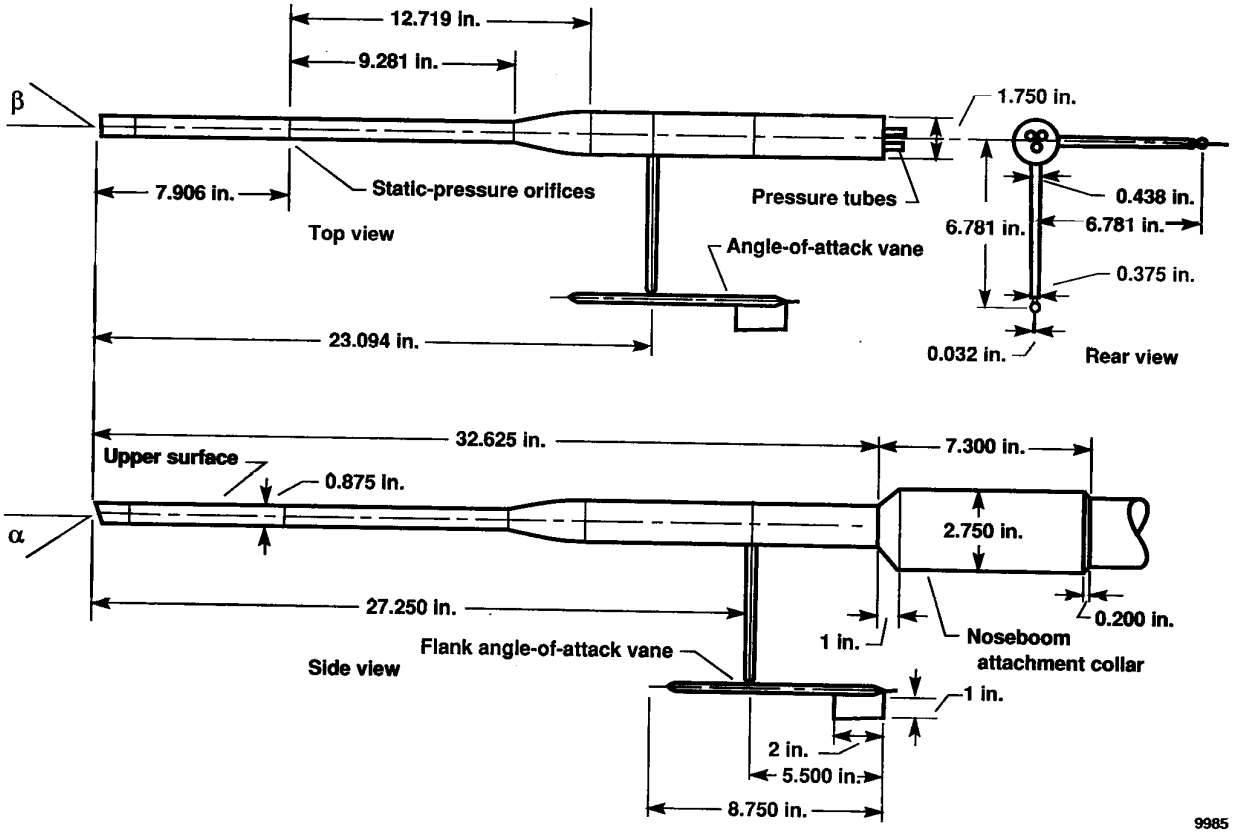

(a) Airdata probe with noseboom attachment collar.

Fig. 2 Standard NACA airdata probe.

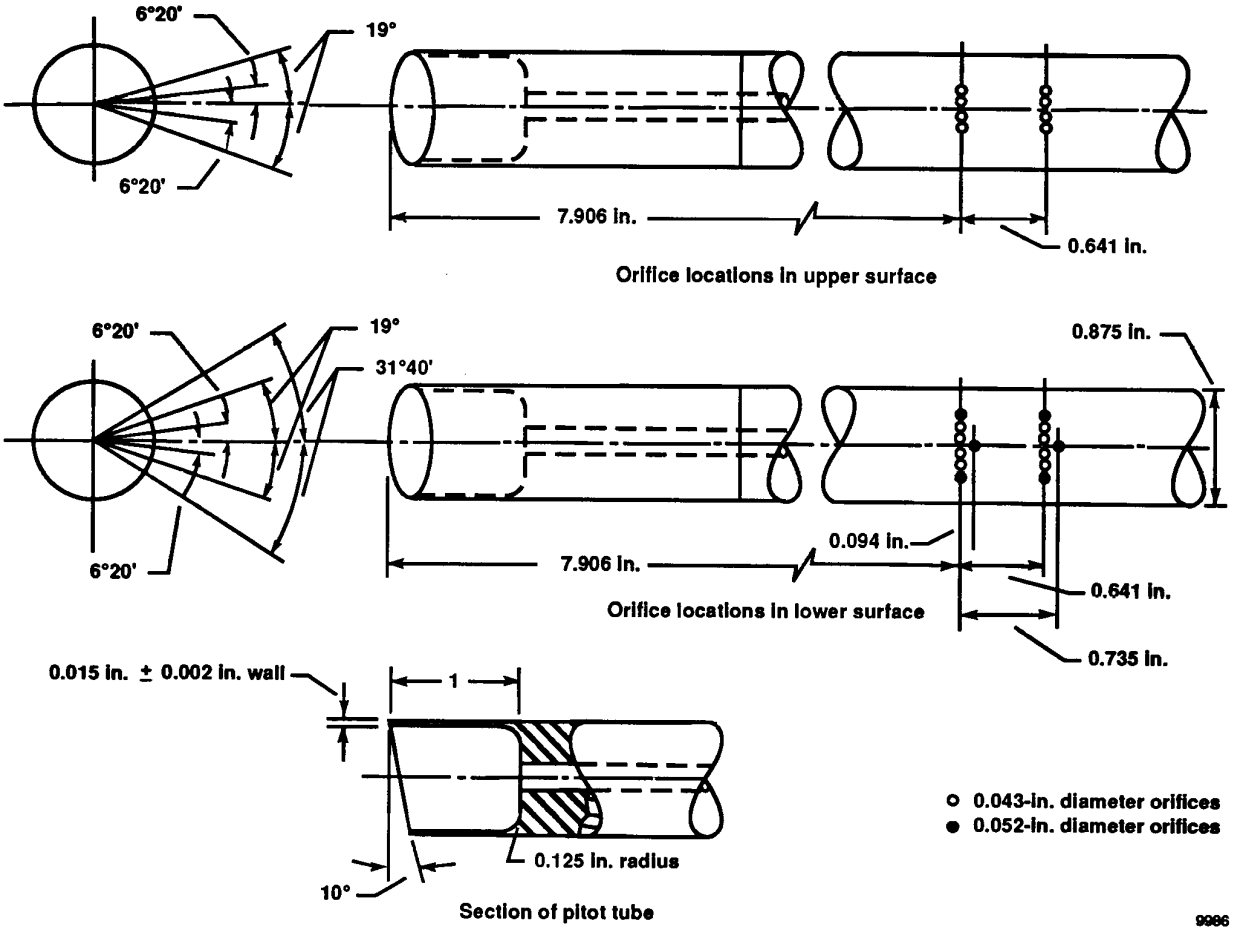

(b) Total and static port configurations.

Fig. 2 Concluded.

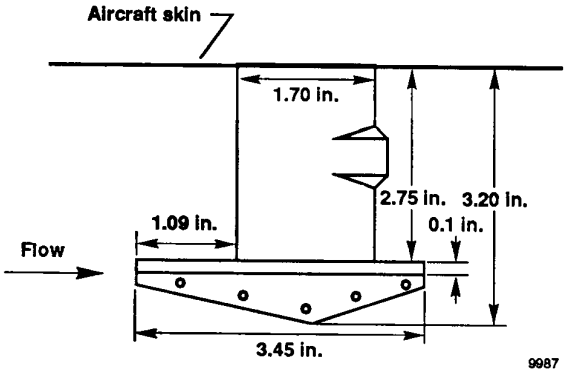

Fig. 3 Nondeiced, open element, total temperature sensor.

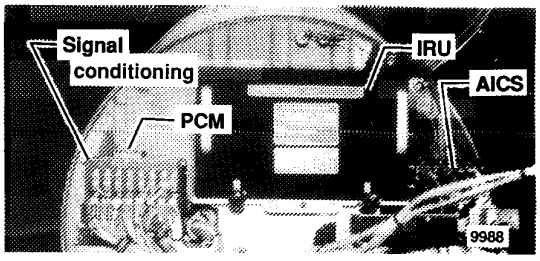

Fig. 4 The IRU, AICS, PCM system, and signal conditioning installed in aircraft.

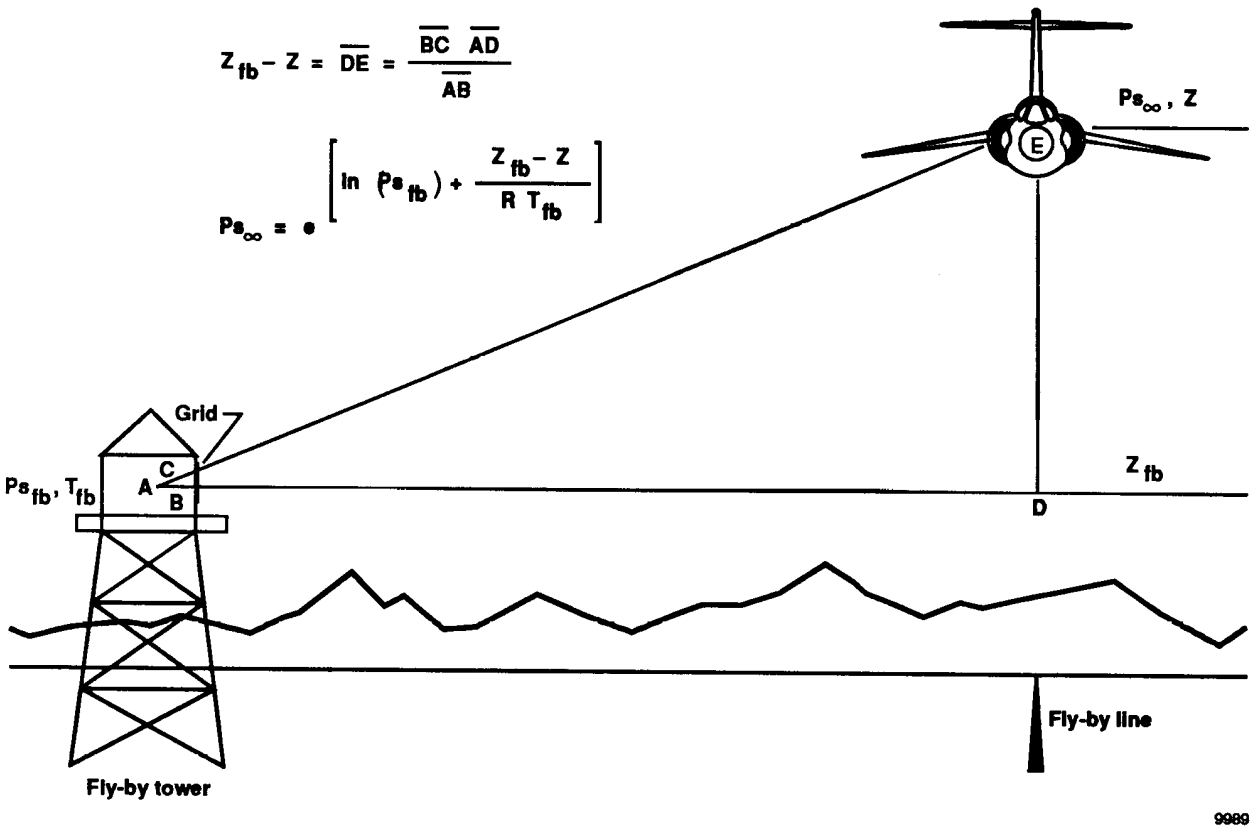

Fig. 5 Tower fly-by position error calibration method.

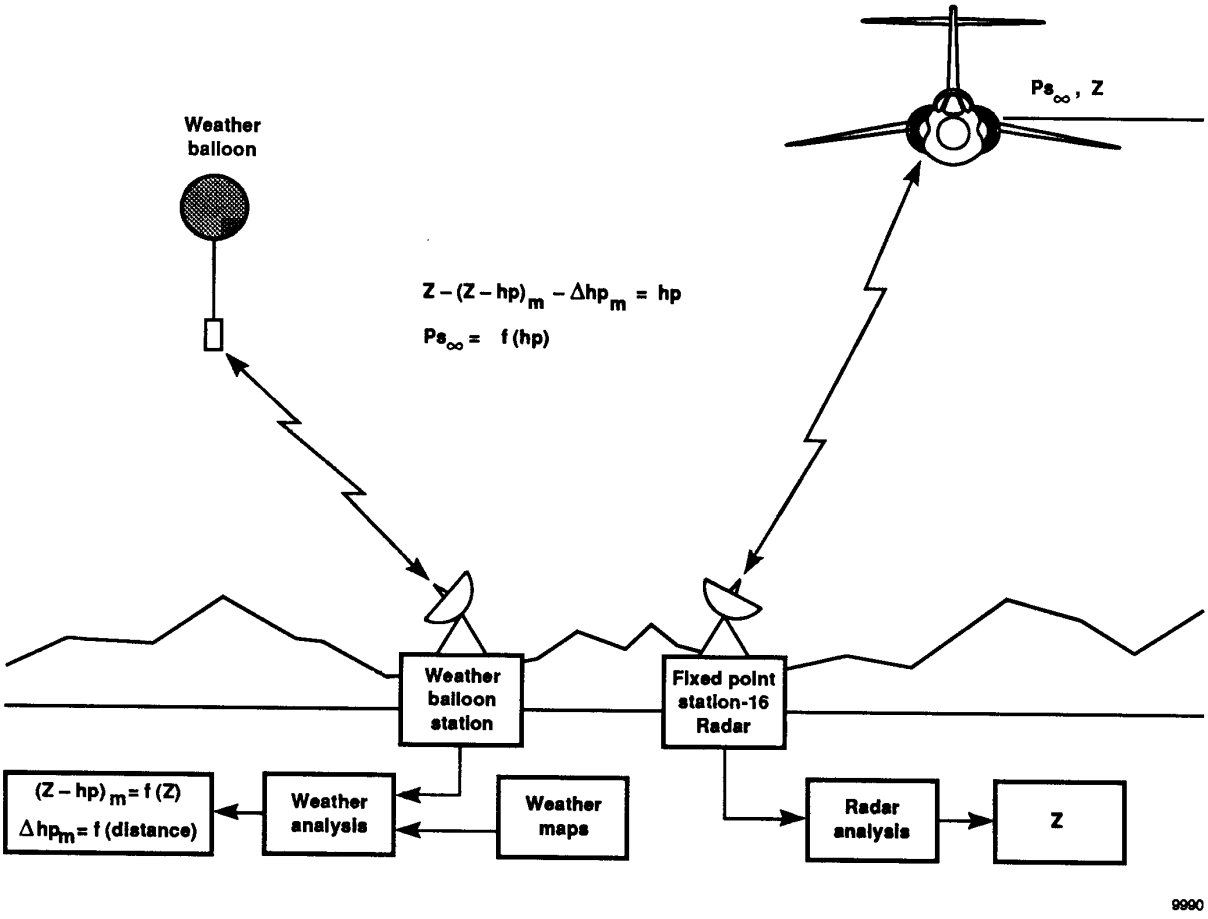

Fig. 6 Radar acceleration-deceleration position error calibration method.

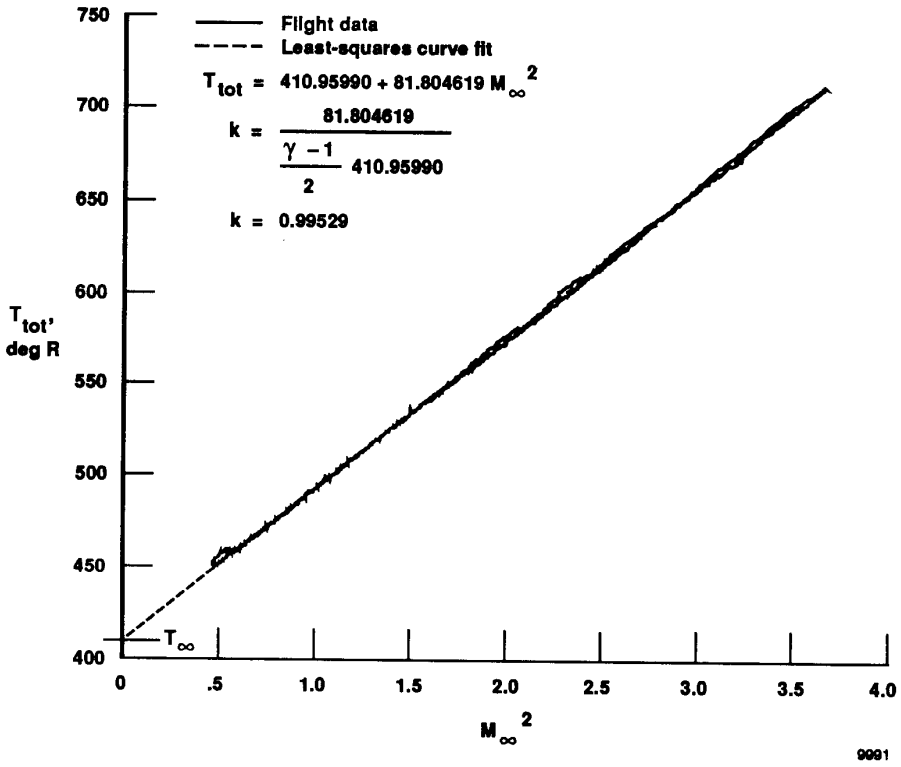

Fig. 7 Total temperature recovery factor calibration technique.

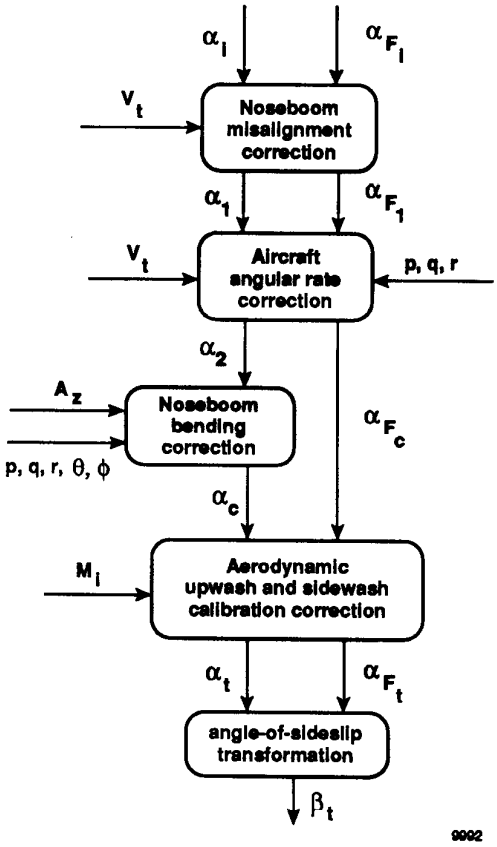

Fig. 8 Flow angle correction steps.

$$\alpha_t = \tan^{-1}\left[\frac{v}{u}\right]$$

$$\alpha_{F_t} = \tan^{-1}\left[\frac{v}{u}\right]$$

$$\beta_t = \sin^{-1}\left[\frac{v}{V_t}\right]$$

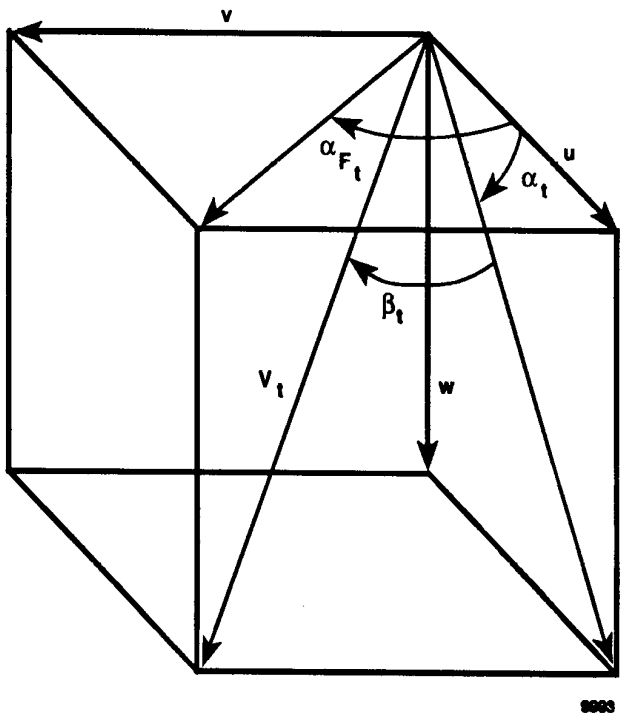

Fig. 9 Flow angle definitions.

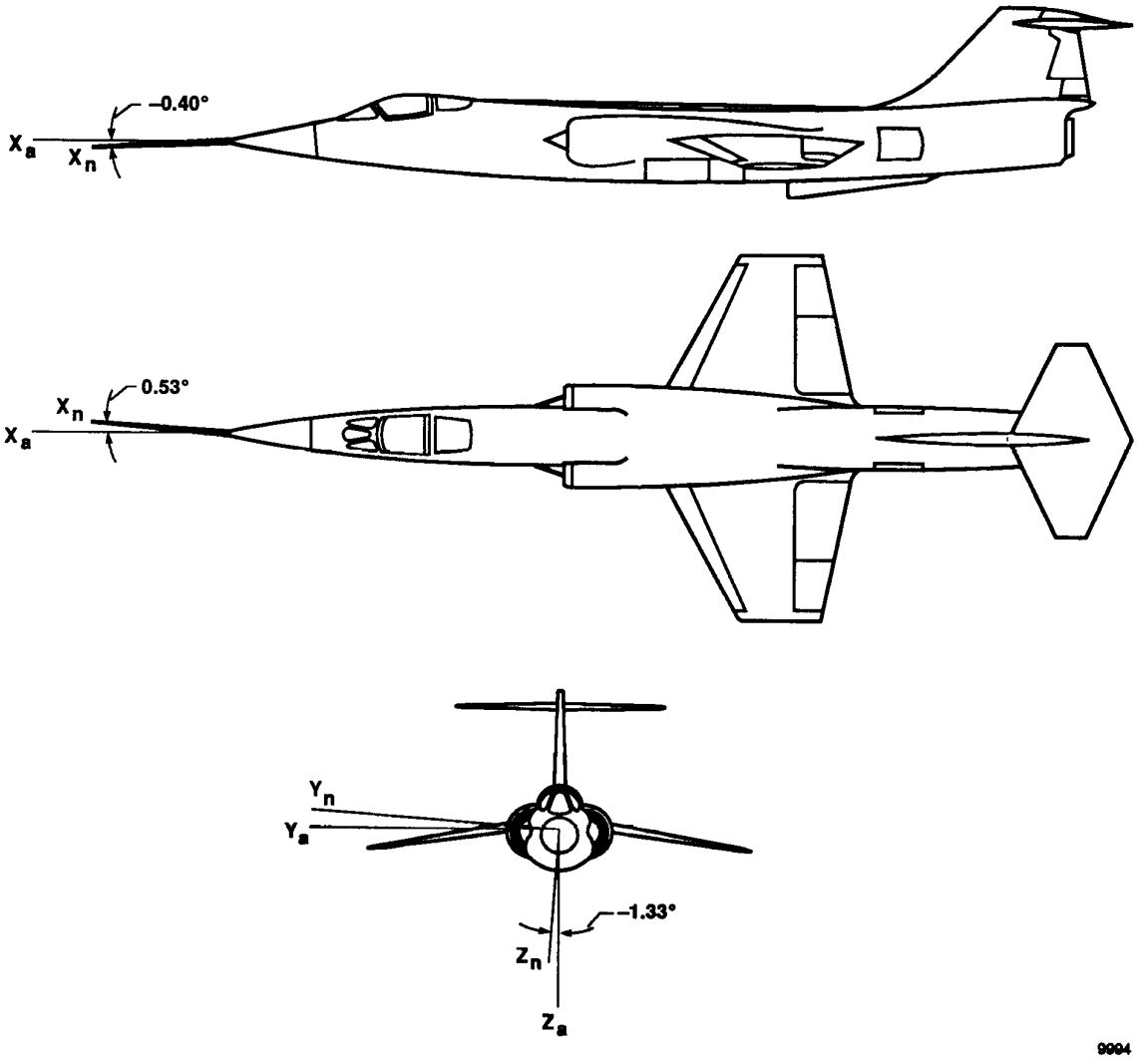

Fig. 10 Noseboom offset angles for check 1.

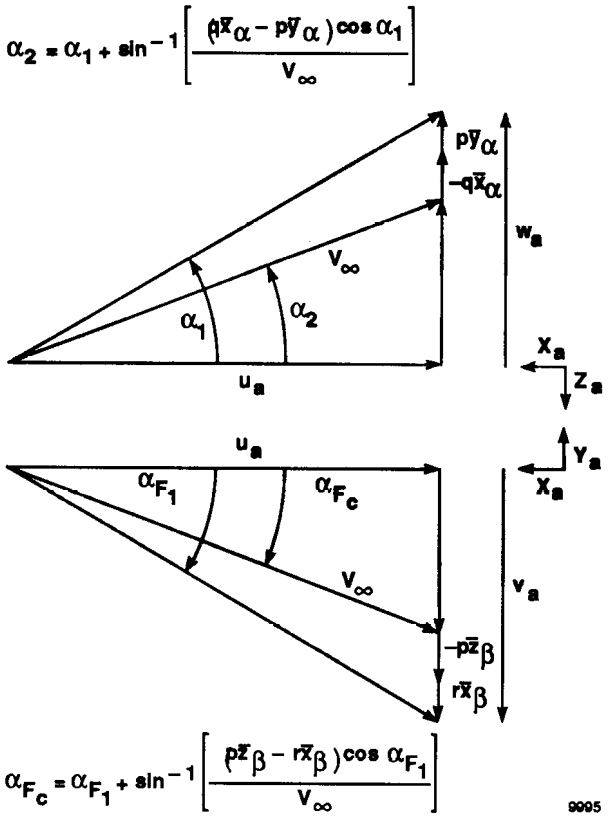

Fig. 11 Flow angle angular rate corrections.

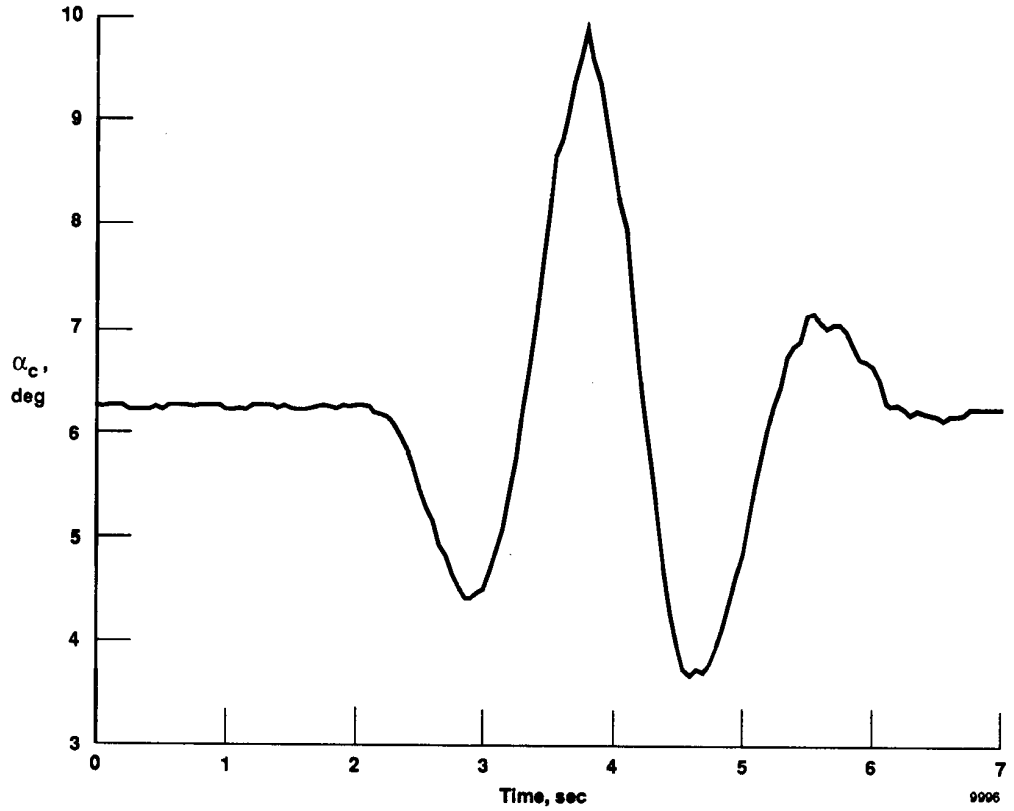

(a) Angle of attack.

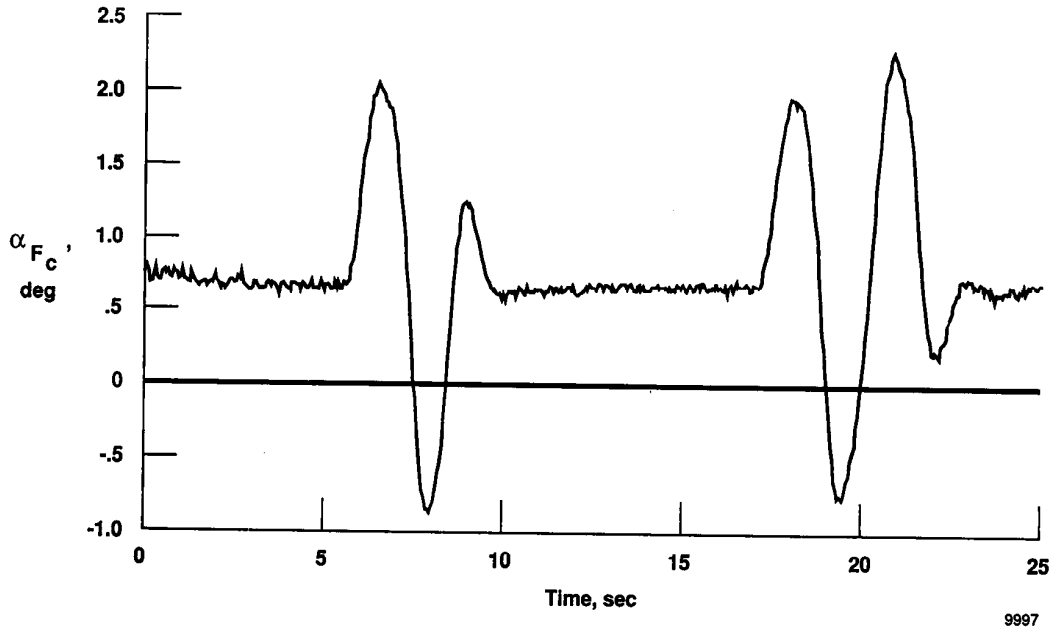

(b) Angle of sideslip.

Fig. 12 Typical subsonic calibration maneuvers at $M_\infty = 0.92$.

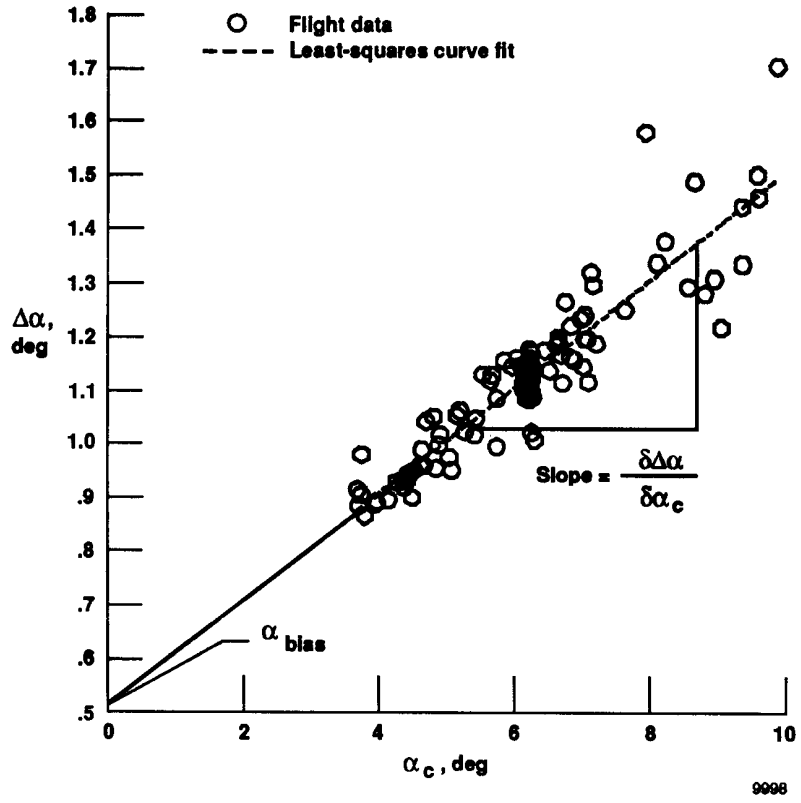

(a) Angle of attack.

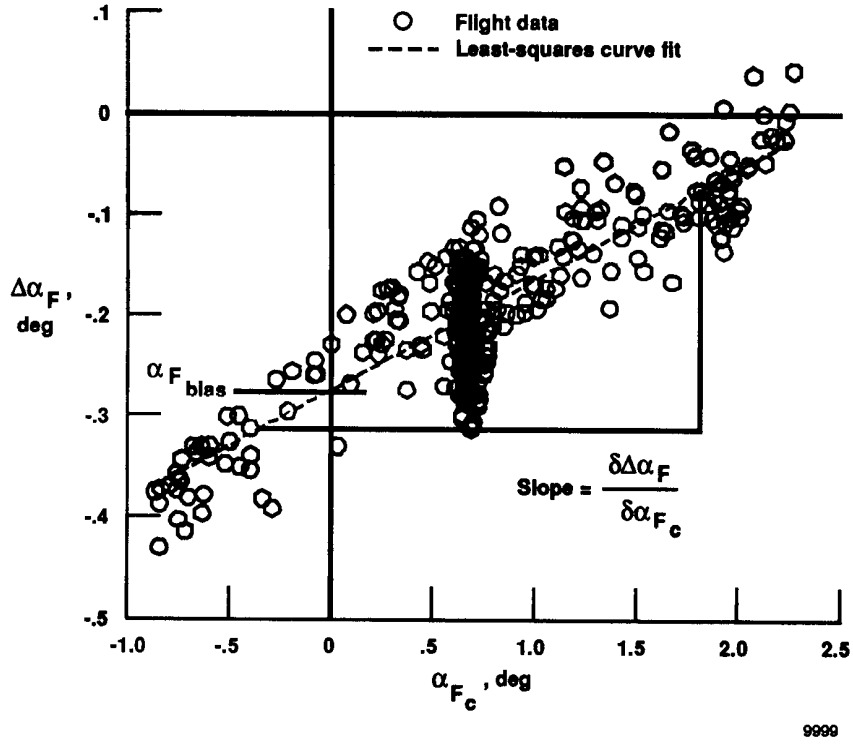

(b) Angle of sideslip.

Fig. 13 Subsonic calibration methods with typical data at $M_\infty = 0.92$.

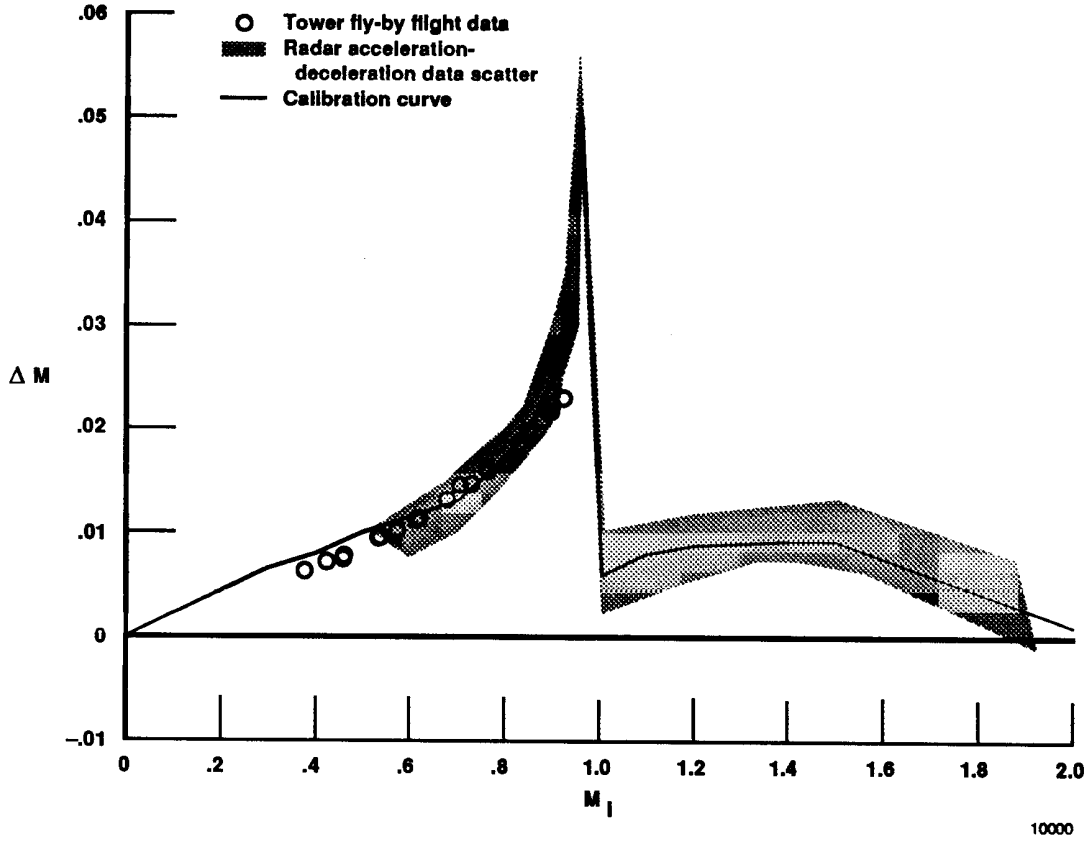

Fig. 14 Mach number position error calibration.

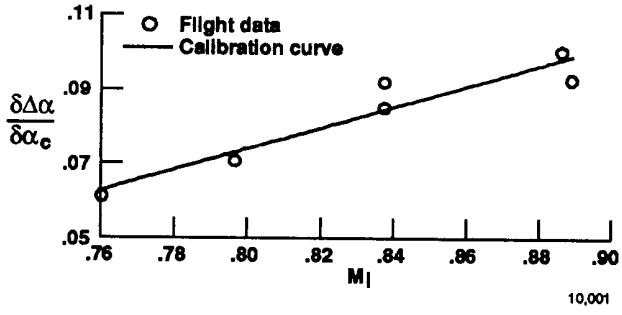

Fig. 15 Subsonic upwash factor.

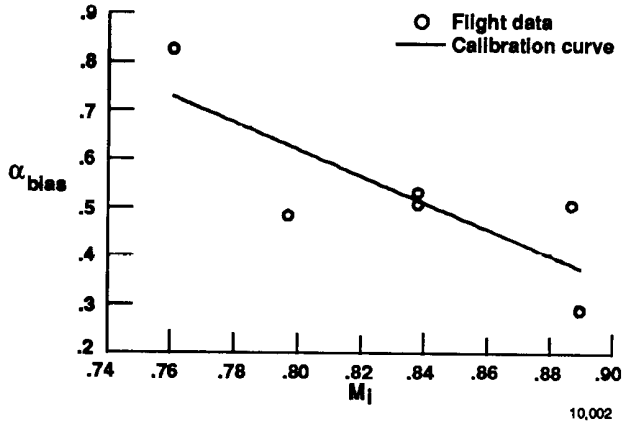

Fig. 16 Subsonic angle-of-attack bias.

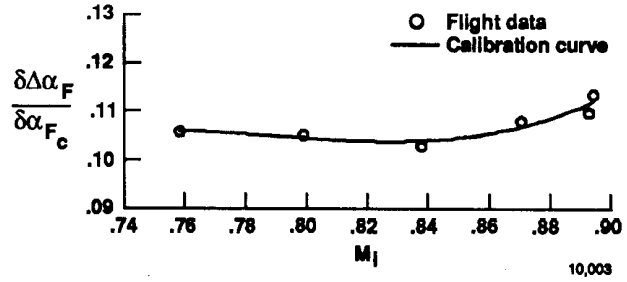

Fig. 17 Subsonic sidewash factor.

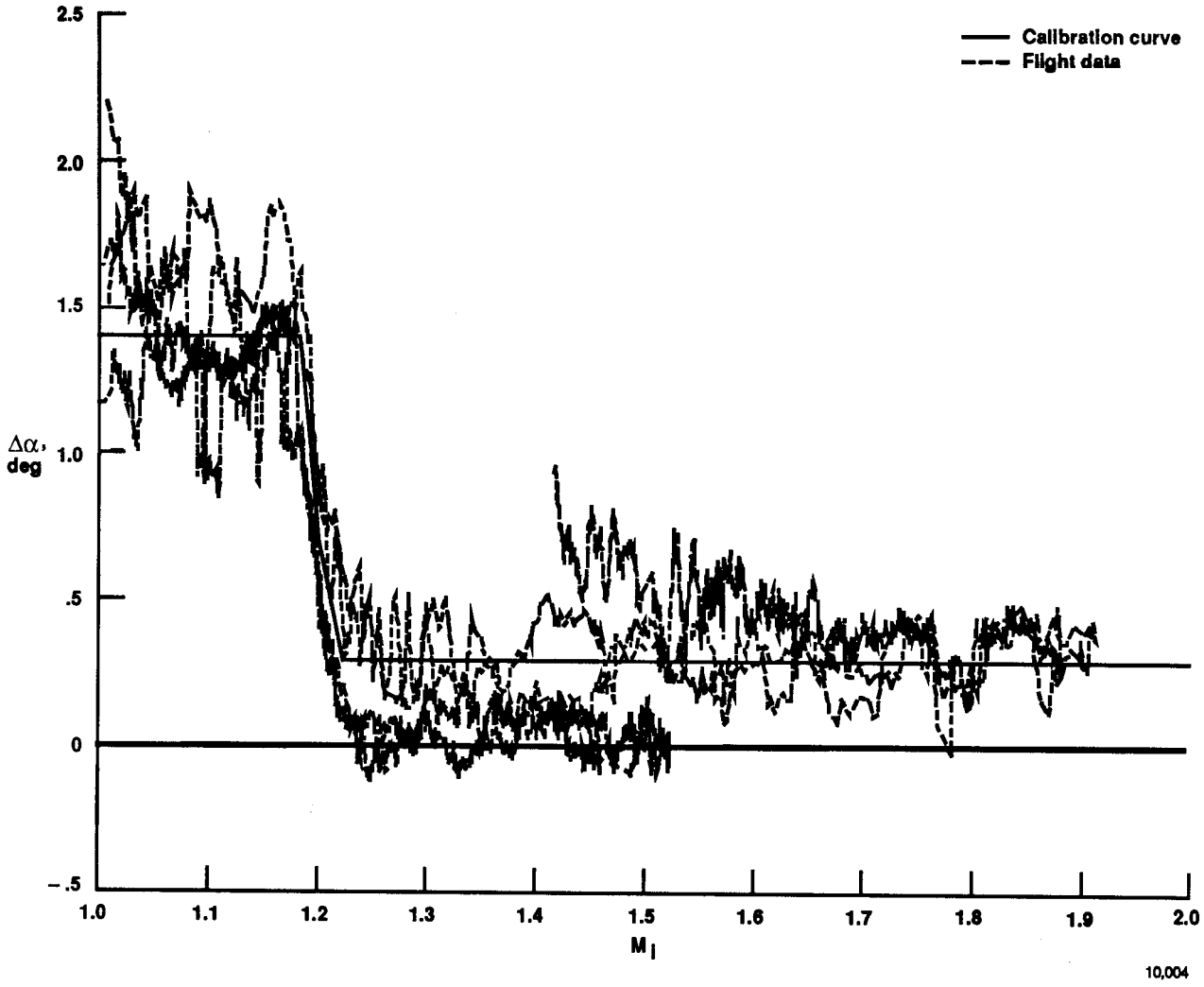

Fig. 18 Supersonic angle-of-attack calibration.

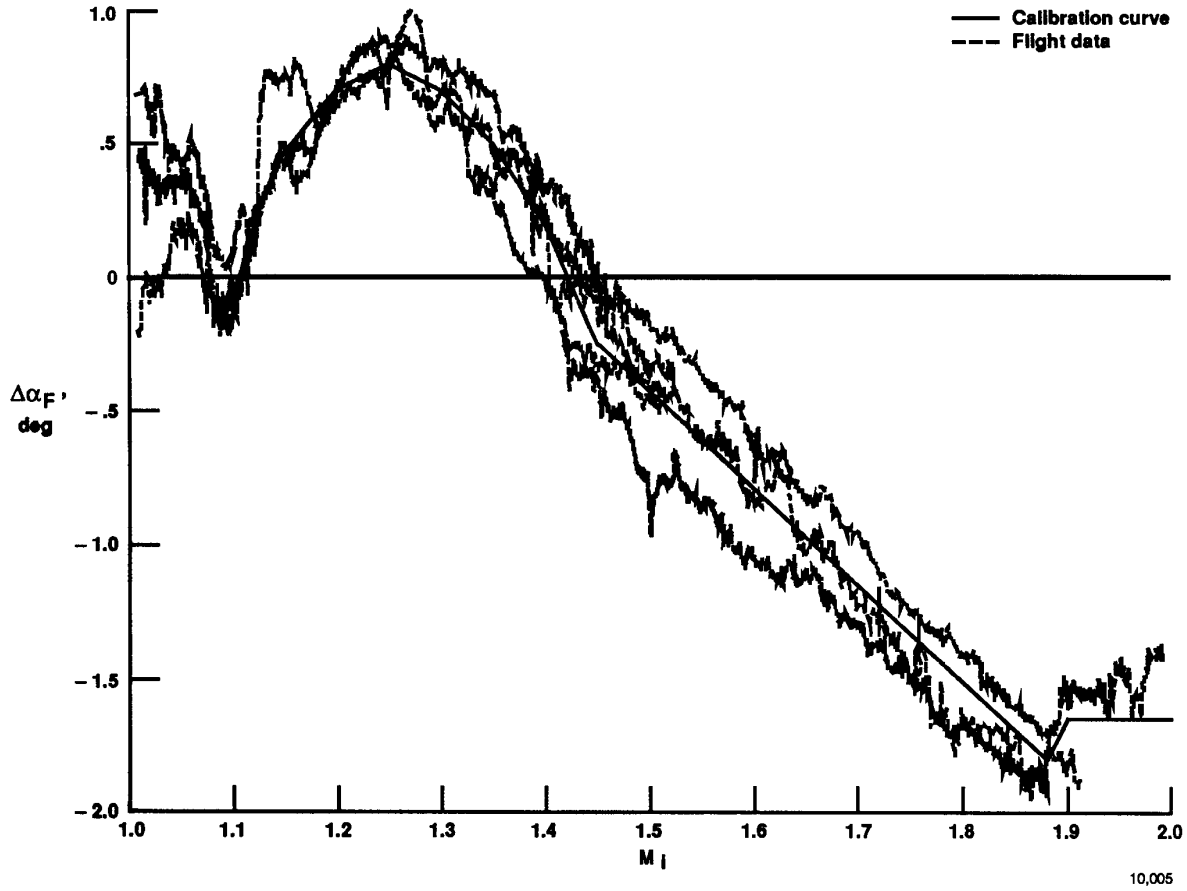

Fig. 19 Supersonic angle-of-sideslip calibration.

NASA
National Aeronautics and Space Administration

Report Documentation Page

1. Report No.	2. Government Accession No.	3. Recipient's Catalog No.
NASA TM-101714		

4. Title and Subtitle

Airdata Calibration of a High-Performance Aircraft for Measuring Atmospheric Wind Profiles

5. Report Date

January 1990

6. Performing Organization Code

7. Author(s)

Edward A. Haering, Jr.

8. Performing Organization Report No.

H-1580

10. Work Unit No.

RTOP 505-68-31

9. Performing Organization Name and Address

NASA Ames Research Center
Dryden Flight Research Facility
P.O. Box 273, Edwards, CA 93523-5000

11. Contract or Grant No.

13. Type of Report and Period Covered

Technical Memorandum

12. Sponsoring Agency Name and Address

National Aeronautics and Space Administration
Washington, DC 20546

14. Sponsoring Agency Code

15. Supplementary Notes

Prepared as AIAA 90-0320 for presentation at AIAA 28th Aerospace Sciences Meeting, Reno, Nevada, January 8–11, 1990.

16. Abstract

The research airdata system of an instrumented F-104 aircraft has been calibrated to measure winds aloft in support of the space shuttle wind measurement investigation at the National Aeronautics and Space Administration Ames Research Center Dryden Flight Research Facility. For this investigation, wind measurement accuracies comparable to those obtained from Jimsphere balloons were desired. This required an airdata calibration more accurate than needed for most aircraft research programs. The F-104 aircraft was equipped with a research pitot-static noseboom with integral angle-of-attack and flank angle-of-attack vanes and a ring-laser-gyro inertial reference unit. Tower fly-bys and radar acceleration-decelerations were used to calibrate Mach number and total temperature. Angle of attack and angle of sideslip were calibrated with a trajectory reconstruction technique using a multiple-state linear Kalman filter. The F-104 aircraft and instrumentation configuration, flight test maneuvers, data corrections, calibration techniques, and resulting calibrations and data repeatability are presented. Recommendations for future airdata systems on aircraft used to measure winds aloft are also given.

17. Key Words (Suggested by Author(s))	18. Distribution Statement
Airdata calibration Trajectory reconstruction Wind measurement	Unclassified — Unlimited Subject category 05

19. Security Classif. (of this report)	20. Security Classif. (of this page)	21. No. of pages	22. Price
Unclassified	Unclassified	27	A03

NASA FORM 1626 OCT 86

**For sale by the National Technical Information Service, Springfield, VA 22161-2171.*